Noise and model uncertainties in ocean color remote sensing

Robert Frouin[a] and Bruno Pelletier[b]

[a]Scripps Institution of Oceanography, University of California San Diego
9500 Gilman Drive, La Jolla, California 92093-224, USA
[b]Department of Mathematics, UMR CNRS 5149, Université Montpellier II
Place Eugène Bataillon, 34095 Montpellier, France

ABSTRACT

The performance of ocean color inversion algorithms is strongly impacted by the various sources of uncertainties, including measurement noise, calibration noise, pre-processing and radiation transfer modeling uncertainties. In this work, an attempt at assessing the overall departure of theory from measurements is conducted based on an in-situ matchup data set. The statistical properties of these differences are first estimated, and are next used to define a Bayesian solution to the inverse problem of atmospheric correction. It is found that there may exist multiple solutions to the inverse problem. The methodology also allows the construction of general confidence domains on the retrieved marine reflectance, without shape restrictions.

Keywords: Ocean Color, Remote Sensing, Statistical Inverse Problems, Noise

1. INTRODUCTION

Top-of-atmosphere (TOA) radiometric measurements over oceans are affected by multiple sources of noise, ranging from purely radiometric noise to calibration issues. Similarly, forward ocean color models, giving a theoretical representation of the satellite signal, are also subject to multiple uncertainties. These include uncertainties coming from pre-processing operations, like correction for molecular effects. These also encompass model uncertainties associated with the definition, and selection, of aerosol models, via their composition, vertical distribution, absorbing and scattering properties. All in all, since atmospheric correction of satellite imagery algorithms are based on these forward models, it is therefore essential to assess the departure of theory from actual measurements. For instance, in a deterministic context, knowledge of the noise magnitude allows to better calibrate the regularization parameter in defining a regularized solution to an ill-posed inverse problem (see e.g., Engl, Hanke, and Neubauer, 1996). In a stochastic setup, where one considers random perturbations of the measurements, knowledge of the noise distribution typically allows to improve the accuracy of the retrievals over a deterministic inversion line. It is also possible in this case to provide an estimate of the distribution of the retrieved parameters, from which confidence domains can be extracted.

In this work, these questions are investigated on a matchup data-set totalizing 97 samples of concomitant measurements of TOA reflectance in the 8 SeaWiFS bands, and in-situ measurements of the marine reflectance, originating from the NOMAD data-set. The samples have been selected to be representative of Case I waters. In a first part, the statistical properties of the differences between the theory and actual measurements are estimated. Because the data-set contains only TOA and marine reflectance spectra, the state of the atmosphere must first be retrieved for each sample, which amounts at solving an inverse problem. That said, since the atmosphere contributes to the majority of the satellite signal, this inverse problem can be considered as well conditioned. For this purpose, we adopted a numerical route by sampling a radiative transfer code on a fine grid.

In a second part, the noise distribution is used to develop an atmospheric correction line in a Bayesian framework. Bayesian methods to ill-posed inverse problems allow to simply account for known constraints by translating a-priori informations into prior distributions. The result of a Bayesian inversion is a probability

Email: rfrouin@ucsd.edu; pelletier@math.univ-montp2.fr.

Ocean Remote Sensing: Methods and Applications, edited by Robert J. Frouin, Proc. of SPIE Vol. 7459, 745905 · © 2009 SPIE · CCC code: 0277-786X/09/$18 · doi: 10.1117/12.829794

distribution on the space of the parameters to be retrieved. Several useful quantities can then be defined from this distribution, like its mean or mode (for pointwise estimates) or confidence domains (for constructing maps of uncertainties). Let us mention that inversion lines based on regression techniques, like neural networks (Gross et al., 2007; Shroeder et al., 2007) or function fields (Pelletier and Frouin, 2006; Frouin and Pelletier, 2007), do converge to the conditional mean (as a function) of the posterior distribution, the definition of which depends both on the sampling distribution and the noise distribution. Hence a "good" choice of priors as well as of noise distribution is essential to the performance of these techniques. At last, to incorporate realistic constraints on the marine reflectance, we developed a model of its distribution, accounting for the average effect the total pigment concentration, and variability thereof.

This note is organized as follows. First, the radiative transfer simulations are presented (Section 2), and the noise estimation procedure is described (Section 3). Next, a short background on Bayesian technique is provided, followed by an analysis from in situ data of the variability of marine reflectance and the exposition and discussion of the atmospheric correction results (Section 4). Finally, conclusions are summarized, and directions for improvements and future work are given (Section 5).

2. RADIATIVE TRANSFER SIMULATIONS

The top-of-atmosphere reflectance, ρ_{TOA}, corrected for molecular effects, is decomposed as

$$\rho_{TOA} = \rho_a + T_a \frac{\rho_w}{1 - S_a \rho_w}, \tag{1}$$

where ρ_a and ρ_w are the atmospheric and marine reflectance, T_a is a transmittance, and S_a and albedo. In practice, the quantities ρ_a, T_a, and S_a are obtained by running a radiative transfer code twice, with and without aerosols. The difference between the results of the two runs allow to evaluate ρ_a. Therefore, ρ_a depends mainly on aerosol content and type, but also depends on whitecaps, and molecular/aerosols coupling.

Using the Successive Order of Scattering (SOS) radiative transfer code, we generated an extensive data set of the atmospheric terms ρ_a, T_a, and S_a. In the simulations, the parameters have been sampled as follows: 3 pressure values, 5 wind speeds, 3 aerosol scale heights, 8 aerosol optical thicknesses (at 865 nm), and 27 aerosol models. The aerosol models are mixtures of maritime, continental, and urban WMO models and Shettle and Fenn (1979) models with varied humidity. The sampling grid leads to about $10,000$ points, per wavelength and viewing configuration, and the calculations have been repeated for $88,000$ viewing configurations.

3. NOISE ESTIMATION

3.1 Methodology

Set x_a equal to the triple (ρ_a, T_a, S_a), and let $\Phi(x_a, \rho_w) = \rho_a + T_a \frac{\rho_w}{1 - S_a \rho_w}$. Our objective is to estimate how far a noisy observation $\rho^\star_{TOA}$ of ρ_{TOA} departs from the range of the operator Φ. To this aim, based on a sample of size n of concomitant observations of the form $(\rho^\star_w, \rho_{TOA})^\star)$, our strategy is to minimize over x_a the error norm $\|\rho^\star_{TOA} - \Phi(x_a, \rho^\star_w)\|$. We define an estimate of x_a as a point $\hat{x}_a$ at which the infimum is attained, i.e.,

$$\|\rho^\star_{TOA} - \Phi(\hat{x}_a, \rho^\star_w)\| = \inf_{x_a} \|\rho^\star_{TOA} - \Phi(x_a, \rho^\star_w)\|, \tag{2}$$

and an estimate of ρ_{TOA} by

$$\hat{\rho}_{TOA} = \Phi(\hat{x}_a, \rho^\star_w).$$

The differences $\rho^\star_{TOA} - \hat{\rho}_{TOA}$ are then taken as a proxy for noise realizations in an additive noise model of the form:

$$\rho^\star_{TOA} = \rho_{TOA} + \varepsilon.$$

Note first that with this procedure, the noise includes measurement noise on ρ_{TOA}, model uncertainties (aerosol models, molecular correction, etc), as well as measurements errors on the marine reflectance, propagated through

Φ. Second, the infimum in (2) may not be attained at a unique point, i.e., $\hat{x}_a$ satisfying (2) need not be unique. However, considering the smoothness of the terms ρ_a, T_a and S_a, if the noise magnitude happens to be small enough, it is likely that $\hat{x}_a$ be actually unique. Third, ideally, assessing differences between the theory (i.e., Φ) and the measurements (i.e., $\rho^\star_{TOA}$) would require simultaneous measurements of both the marine and atmospheric terms (i.e., x_a and ρ_w). This ideal setup is clearly out of reach. Therefore, the only workaround is to first estimate x_a, as exposed above. As a consequence, the actual differences between theory and TOA measurements are necessarily larger. On the other hand, since (i) ρ_a is the leading term in (1), and since (ii) the set $\{\rho_a\}$ is smooth, the problem of reconstructing x_a from a pair of observations $(\rho^\star_w, \rho^\star_{TOA})$ is likely to be very well conditioned.

3.2 Results

The methodology has been applied to a sample of size $n = 97$ of pairs $(\rho^\star_w, \rho^\star_{TOA})$. The TOA reflectance originates from the SeaWiFS sensor and have been corrected for molecular effects, leading to $\rho^\star_{TOA}$. The marine reflectance $\rho^\star_w$ is extracted from the NOMAD data set (Werdell and Bailey, 2005). The difference in date and location between $\rho^\star_w$ and $\rho^\star_{TOA}$ is small (a few hours).

Estimated versus measured TOA reflectance (i.e., $\hat{\rho}_{TOA}$ vs $\rho^\star_{TOA}$) is displayed wavelength-wise in Figure 5. The differences are found to be almost unbiased, with moderate dispersion. The size of the sample ($n = 97$) is too small, though, to assess correlations, and possible dependence of the noise magnitude with respect to the input parameters of the operator. But marginal (i.e., per wavelength) histograms of the differences are essentially symmetrical (around 0), so that a Gaussian noise model with diagonal covariance matrix can be taken as a workable noise model. In fact, the marginal distributions of the differences appear more concentrated than a Normal distribution. So assuming a Gaussian noise is a conservative hypothesis. In conclusion, the noise ε is assumed to follow a Normal distribution with mean 0 and covariance matrix $\Sigma = \mathrm{diag}(\sigma_1^2, \ldots, \sigma_8^2)$, where the σ_i's are the estimated standard deviations of the 8 components of the differences.

4. BAYESIAN INFERENCE

4.1 Background

As opposed to deterministic regularization methods of inverse problems (see e.g., Engl, Hanke, and Neubauer, 1996), in the Bayesian approach, all free parameters are considered as random objects. A solution to the inverse problem is obtained in the form of a probability distribution, called the posterior distribution, or distribution a-posteriori. Pointwise estimates can then be formed from the posterior distribution as the mean, the mode, the L^1-median, etc. Additionally, confidence domains can also be constructed from the posterior distribution.

Recall that in our setup, we observe $\rho^\star_{TOA} = \Phi(x_a, \rho_w) + \varepsilon$. The quantities required to construct the posterior distribution are: (i) a *noise distribution* P_ε, a *prior distribution* on the atmosphere P_a, and a *prior distribution* on the marine reflectance P_w. In the case where P_ε, P_a, and P_w admits densities f_ε, f_a, and f_w with respect to the Lebesgue measure the *posterior distribution* $Q(\mathrm{d}\rho_w|\rho^\star_{TOA})$ of ρ_w given $\rho^\star_{TOA}$ is defined by

$$\begin{aligned} Q(\mathrm{d}\rho_w|\rho^\star_{TOA}) &= \frac{\int f_\varepsilon\left(\rho^\star_{TOA} - \Phi(x_a, \rho_w)\right) f_a(x_a)\mathrm{d}x_a}{\int f_\varepsilon\left(\rho^\star_{TOA} - \Phi(x_a, \rho_w)\right) f_a(x_a)\mathrm{d}x_a f_w(\rho_w)\mathrm{d}\rho_w} f_w(\rho_w)\mathrm{d}\rho_w \\ &:= q(\rho_w|\rho^\star_{TOA})\mathrm{d}\rho_w, \end{aligned}$$

but $Q(\mathrm{d}\rho_w|\rho^\star_{TOA})$ can also be expressed directly from the measures P_ε, P_a, and P_w, which need not be absolutely continuous. As exposed above, pointwise estimates $\hat{\rho}_w$ of ρ_w can be extracted from the posterior distribution, like the mean $\hat{\rho}_w = \int \rho_w Q(\mathrm{d}\rho_w|\rho^\star_{TOA})$ or a global mode $\hat{\rho}_w \in \arg\max q(\rho_w|\rho^\star_{TOA})$. To implement this methodology, P_ε can be taken as a multivariate normal distribution with mean zero and diagonal covariance matrix, as exposed in the previous section. There remains to determine "good" priors P_a and P_w for the atmospheric and marine terms. These distributions should reflects the natural variability of x_a and ρ_w, i.e., the likelihood of encountering particular values. The study of the marine reflectance variability is the subject of the next subsection.

In addition to pointwise estimates, the Bayesian framework also allows to construct confidence domains on the retrievals. Specifically, a confidence domain can be defined as a level set of the posterior density $q(\rho_w|\rho^\star_{TOA})$, i.e., as the set of ρ_w for which q is greater than a given threshold $t > 0$. In practice, t has to be selected such that the level set has a pre-specified probability content, typically close to 1, e.g., 0.75 or 0.9.

4.2 Modeling of the marine reflectance variability

We considered the second version of the NOMAD data set, and extracted in-situ measurements of the marine reflectance in the first six channels of the SeaWiFS sensor. The data set contains up to around 4,000 points in some bands. As is well-known, ρ_w strongly depends on the total pigment concentration, further denoted by *chl*. This dependence is visible both on the conditional mean and conditional variance. A preliminary inspection of the data reveals that the conditional variance of ρ_w is better stabilized by a logarithmic transform. The present analysis is therefore based on $\log(\rho_w)$. In a first step, the conditional mean and variance of the components of $\log(\rho_w)$ are estimated using smoothing splines. The results at 412 and 443 nm are displayed in Figure 5, top. Histograms of the standardized residuals are represented in Figure 5, bottom, i.e., the differences between $\log(\rho_w)$ and the estimated mean, divided by the estimated standard deviation. While standard statistical tests reject the assumption of Normality, assuming that the residuals are normally distributed still remains a reasonable assumption (see Figure 5, bottom), considering that in-situ measurements may be noisy. In a second step, the correlations between the standardized residuals are estimated in the form of a fixed covariance matrix (not depending on *chl*). Putting all pieces together, we end up with the model

$$\log(\rho_w) = \mu(chl) + \Sigma(chl)\varepsilon,$$

where ε follows a multivariate Normal distribution with mean 0 and covariance matrix equal to the identity of $\mathbb{R}^6$. Equivalently, this model specifies that ρ_w given *chl* follows a log-Normal distribution, further denoted by log-$\mathcal{N}(\mu(chl), \Sigma(chl))$, with mean $\mu(chl)$ and covariance matrix $\Sigma(chl)$. The estimation of μ and Σ have been conducted in two steps due to missing values at some components of the in the in-situ marine reflectance. Indeed, μ and Σ could have been estimated simultaneously, but on the subset of the data containing no missing values, thereby discarding a significant number of samples, and thus, increasing estimation error. At last, one can estimate the distribution P_{chl} of *chl* using a kernel density estimator for instance. The marginal distribution of ρ_w is hence obtained by integration of the log-normal density against P_{chl}.

4.3 Inversion results

We evaluated the Bayesian inversion line on the 97 sample points described in section 3.2. The noise distribution P_ε is taken as a multivariate normal distribution with diagonal covariance matrix whose entries are the estimated variances of the noise, as exposed in Section 3.2. The prior distribution of ρ_w is taken as the one constructed in Section 4.2. At last, the atmospheric prior distribution P_a is taken as a uniform distribution over the simulated atmospheric sample (see Section 2). The mean of the posterior distribution is taken as an estimate of the marine reflectance. Estimated versus in-situ marine reflectance are displayed in Figure 5 (top), and similar plots for SeaDAS retrievals are given in Figure 5 (bottom). Root mean squared errors (RMS) are given in Table 4.3, and mean absolute relative errors in Table 4.3. The retrievals are found to be comparable with the SeaDAS ones.

Examples of posterior distributions are given in Figure 5, as well as the construction of a (marginal) confidence domain. For a large proportion of samples, the posterior distributions are highly concentrated, and in-situ values are included in confidence regions at 90%. In some cases, though, the posterior distribution is found to be bi-modal, which is evidence of two distinct solutions to the inverse problem. One example of such a distribution is displayed in Figure 5, bottom. In this situation, the mean of the posterior distribution is clearly not a good estimate (see Figure 5, bottom, left). Instead, the first and second mode of the posterior distribution are potential solutions. For this case, the TOA, atmospheric, and marine reflectance corresponding to the first and second mode are represented in Figure 5. It can be seen that the differences between the TOA spectra are relatively small. This example shows that, in this case, there exists two different pairs $(x_a^{(1)}, \rho_w^{(1)})$ and $(x_a^{(2)}, \rho_w^{(2)})$ such that $\Phi(x_a^{(1)}, \rho_w^{(1)})$ and $\Phi(x_a^{(2)}, \rho_w^{(2)})$ are both close to the measurement $\rho^\star_{TOA}$.

Table 1. Root Mean Square Errors ($\times 10^{-3}$).

λ (nm)	412	443	490	510	555
SeaDAS	5.69	3.89	3.14	2.90	2.43
Bayes	4.86	3.65	3.20	2.73	2.11

Table 2. Mean Absolute Relative Errors (%).

λ (nm)	412	443	490	510	555
SeaDAS	33.24	23.46	18.27	19.48	22.92
Bayes	27.56	22.15	18.28	18.21	19.88

These results have been obtained by endowing the space of TOA reflectance with the L_2 norm, i.e., given two spectra ρ_1 and ρ_2, we have $\|\rho_1 - \rho_2\|^2_{L_2} = \int (\rho_1(\lambda) - \rho_2(\lambda))^2 \, \mathrm{d}\lambda$, where λ denotes the wavelength. Naturally in practice, the integral is approximated by a finite sum of squared differences, with appropriate weights. This choice of norm is somewhat arbitrary and has been retained for convenience. Let us emphasize, though, that changing the norm on space of TOA reflectance can modify the results to some extent. Consider again the plots in Figure 5 where multiple solutions are found. It is apparent that the slope of the TOA spectra in the near infra-red are slightly different. Since variations of slope in the near infra-red are mainly due to aerosol models, it may be more appropriate to select a norm accounting for derivative, like for instance the Sobolev norm

$$\|\rho_1 - \rho_2\|^2_{W_2} = \int (\rho_1(\lambda) - \rho_2(\lambda))^2 \, \mathrm{d}\lambda + \int (\rho_1'(\lambda) - \rho_2'(\lambda))^2 \, \mathrm{d}\lambda, \tag{3}$$

which measures differences on the derivative, in addition to differences in the values of the spectra. Using this type of norm requires a change of reference measure in the additive noise model, to simplify the implementation. Moreover, it is also necessary to consider a weighted version of the W_2 norm, to balance the numerical values of the two terms in (3). Letting these technicalities aside, it is found that the error on the retrievals is slightly decreased, compared with the use of the L_2 norm. But in some cases, multiple solutions are still exhibited.

5. CONCLUSIONS AND PERSPECTIVES

A first step has been made towards assessing the departure of theory from actual satellite measurements, and its consequences on atmospheric correction over Case I waters. The developed methodology allows to incorporate known constraints on the marine reflectance (i.e., correlations between components), and to account for the various sources of uncertainties. By taking the mean of the marine reflectance posterior distribution, the inversion results are found to slightly improve retrievals of marine reflectance compared with SeaDAS estimates, yet the improvement is not significant. On the other hand, the methodology allows the construction of reliable multi-dimensional confidence domains on the retrieved marine reflectance. These confidence domains are specific to each sample and can be constructed for any probability value. Interestingly, it is also found that multiple solutions can arise in some cases, and that they can be detected by tracking the local modes of the posterior distribution. These multiple solutions appear to be isolated (i.e., corresponding to local modes of the posterior distribution), which may originate from the discrete sampling of aerosol models.

Note, finally, that the study has been conducted on a limited number of points ($n = 97$). A better assessment of noise, and its impact on the retrievals like the appearance of multiple solutions, would require further investigations on a sample of larger size. Improvements may certainly be also obtained by reducing sampling errors on the atmospheric terms by interpolation. Considering a continuum of aerosol models would reduce the number of local modes of the posterior distribution, i.e., the posterior distribution would be smoothed. While this is fairly simple to implement when dealing with scalar parameters, the case of aerosol model indices is not straightforward and will deserve some thoughts. Another direction would be to fit a model for the marine reflectance distribution specific to Case I waters.

ACKNOWLEDGMENTS

Funding for this work has been provided by the National Aeronautics and Space Administration under grants NNG05GR20G and NNX08AF65A. The technical support of Mr. John McPherson, Scripps Institution of Oceanography, University of california at San Diego, is gratefully acknowledged.

REFERENCES

1. Shettle, E. P., and Fenn, R. W. (1979). Models for the aerosols of the lower atmopshere and the effect of the humidity variations on their optical properties. Tech. Rep. TR–79–0214, Air Force Geophys. Lab., Bedford,Mass.
2. Engl, H.W., Hanke, M., and Neubauer, A. (1996). *Regularization of Inverse Problems*. Vol. 375 of Mathematics and its Applications. Kluwer Academic Publishers Group, Dordrecht.
3. Werdell, P.J., and Bailey, S. W., 2005: An improved bio-optical data set for ocean color algorithm development and satellite data product validation. *Remote Sensing of Environment*, **Vol. 98**, 122-140.
4. Pelletier, B., and Frouin, R. (2006). Remote Sensing of Phytoplankton Chlorophyll-a Concentration by use of Ridge Function Fields. *Applied Optics*, **Vol. 45**, pp. 784-798.
5. Frouin, R., and Pelletier, B. (2007). Fields of non-linear regression models for atmospheric correction of satellite ocean-color imagery. *Remote Sensing of the Environment*, **Vol. 111**, pp. 450-465.
6. Schroeder, T., Behnert, I., Schaale, M., Fischer, J., and Doerffer, B. (2007). Atmospheric correction algorithm for MERIS above case-2 waters.*International Journal of Remote Sensing*, **Vol. 28**, No. 7, 1469-1486.
7. Gross-Colzy, L., Colzy, S., Frouin, R., and Henry, P. (2007). A general Ocean Color Atmospheric correction scheme based on principal component analysis Part I: Performance on Case 1 and Case 2 waters. In *Coastal Ocean Remote Sensing*, Proceedings of SPIE, **Vol. 6680**, Published by SPIE–The International Society for Optical Engineering, Bellingham, Washington, USA, doi: 10.1117/12.738508, 12 pp.

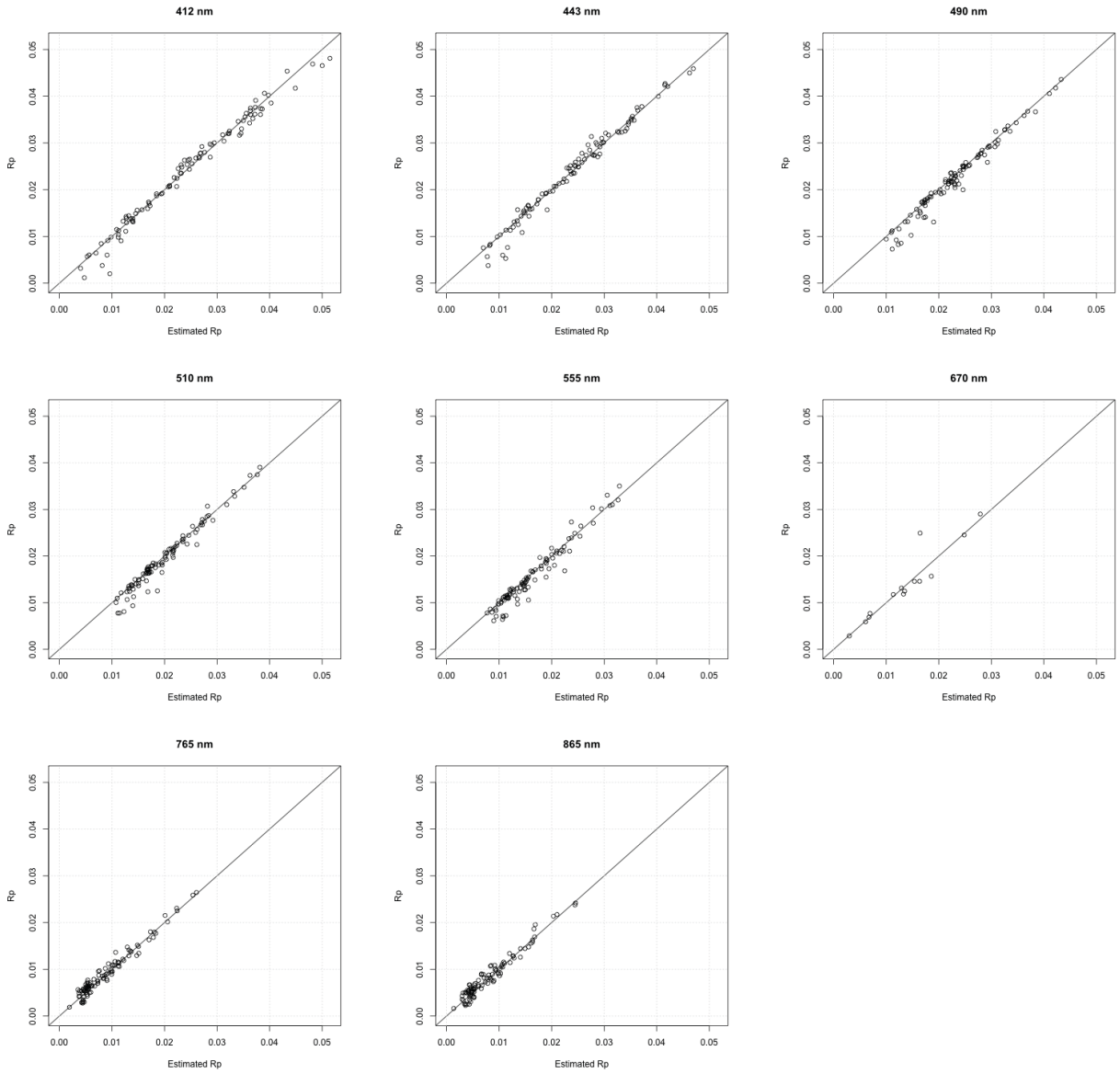

Figure 1. Measured versus estimated TOA reflectance. The number of samples is 97, except for the channel at 670 nm, due to missing values in the in-situ marine reflectance at this wavelength.

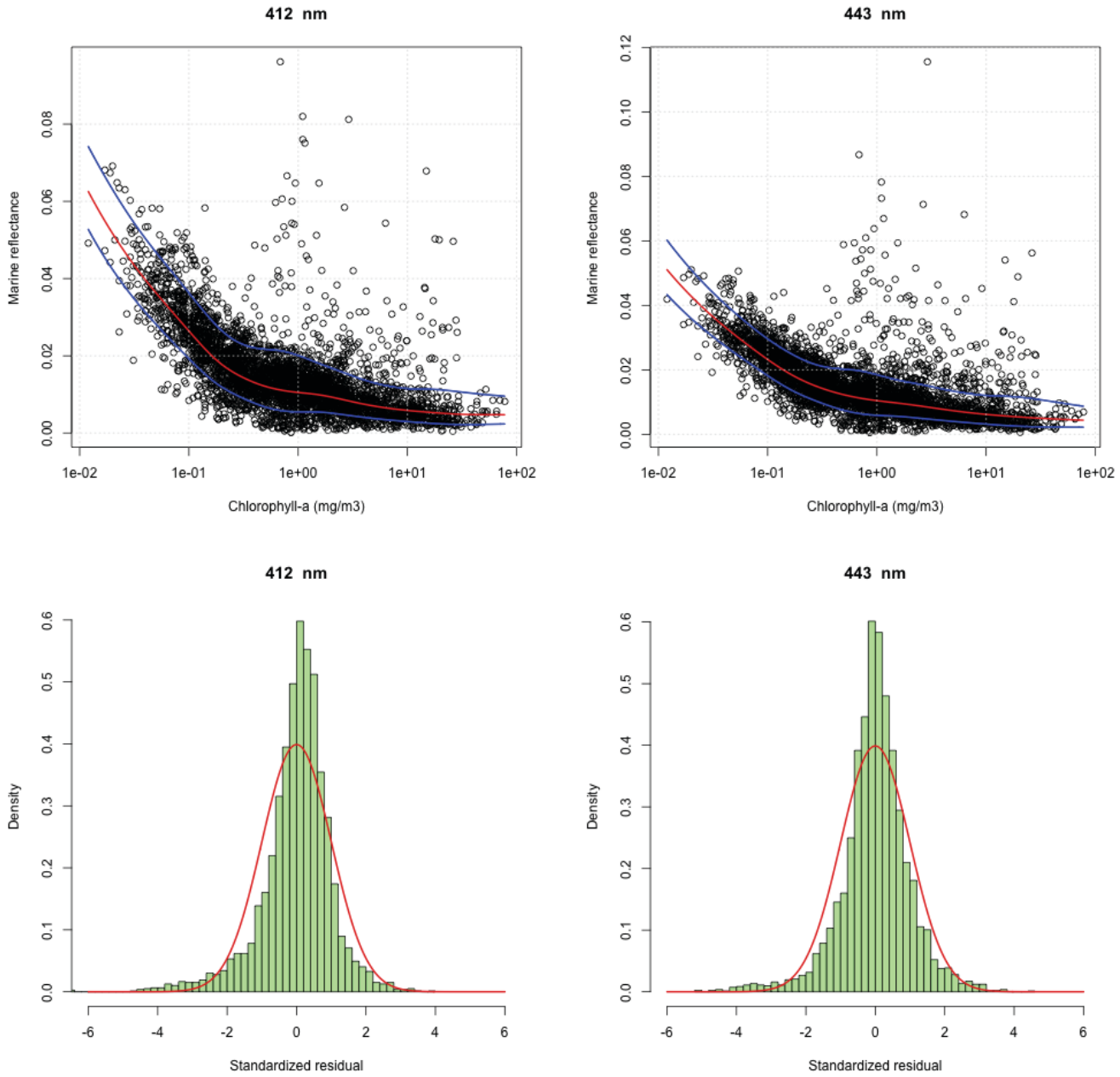

Figure 2. Model of the marine reflectance variability extracted from the NOMAD data set, at 412 and 443 nm. Top: estimated conditional mean of ρ_w given chl (red curve), plus and minus the conditional standard deviation (blue curves). Bottom: standardized residuals histograms with the density of $\mathcal{N}(0,1)$ superimposed (red curve).

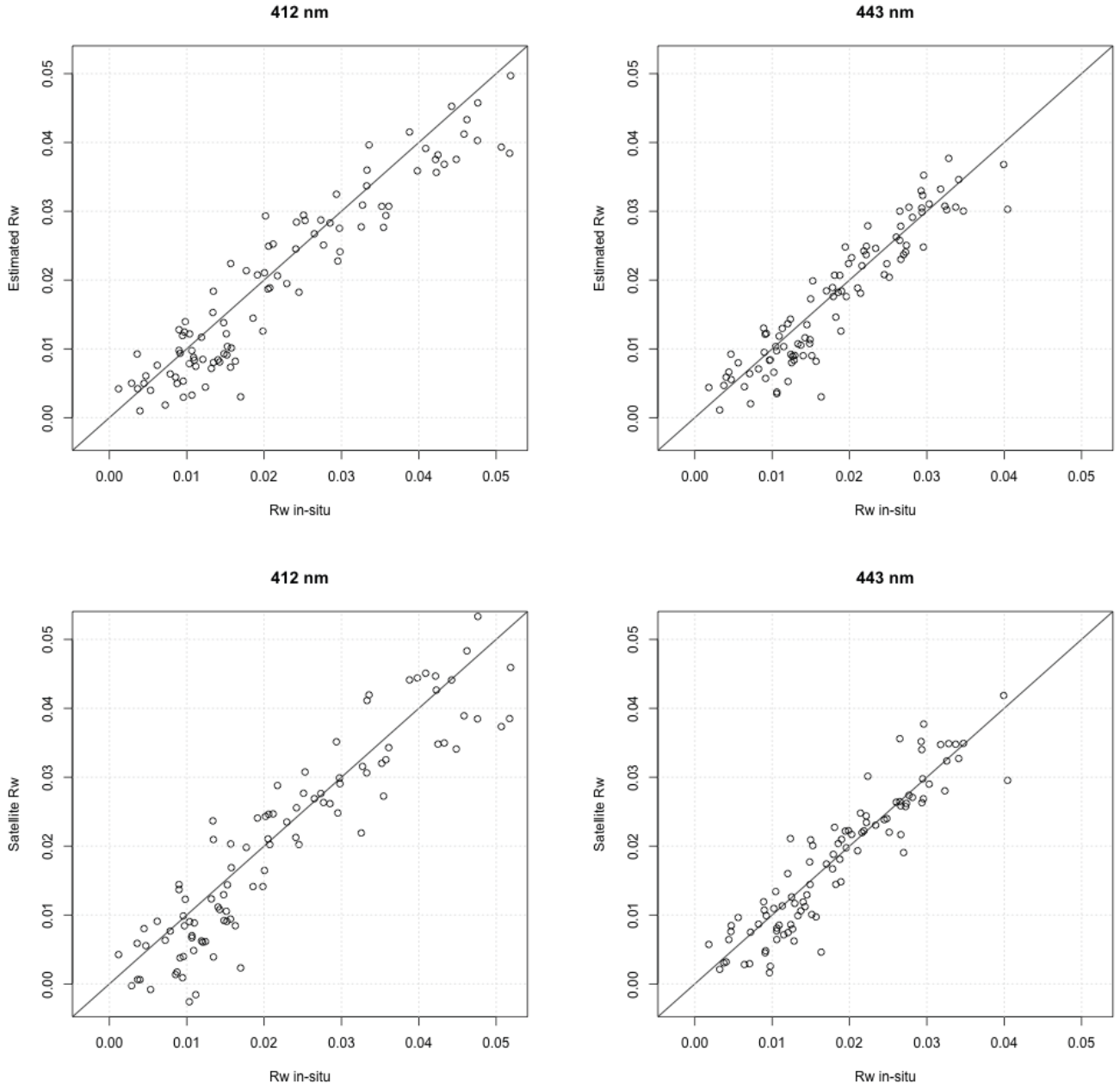

Figure 3. Estimated versus in-situ marine reflectance, at 412 and 443 nm. Top: estimation by the mean of the posterior distribution of ρ_w, constructed using the Sobolev norm, and priors on τ_a and aerosol models. Bottom: SeaDAS estimates.

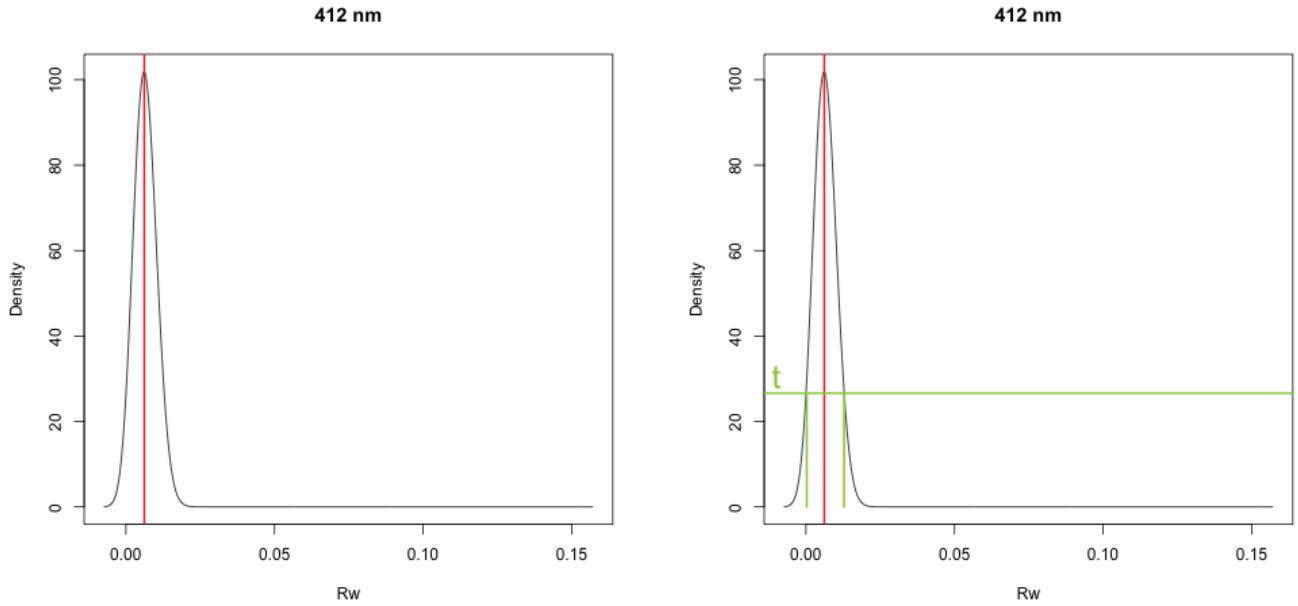

Figure 4. Examples of posterior distributions. Top: example of a favorable situation. The marginal posterior distribution of $\rho_w(412)$ is unimodal, and highly concentrated around the in-situ value (red). In this case, $\rho_w(412)$ is retrieved with negligible error. A confidence domain can be defined as a level set (top-right plot). Bottom: example of non unimodal posterior distribution. The marginal posterior distribution of $\rho_w(412)$ is bimodal, which is evidence of two solutions. Bi-modality is still present on the joint distribution of $(\rho_w(412), \rho_w(443))$ (bottom-right plot).

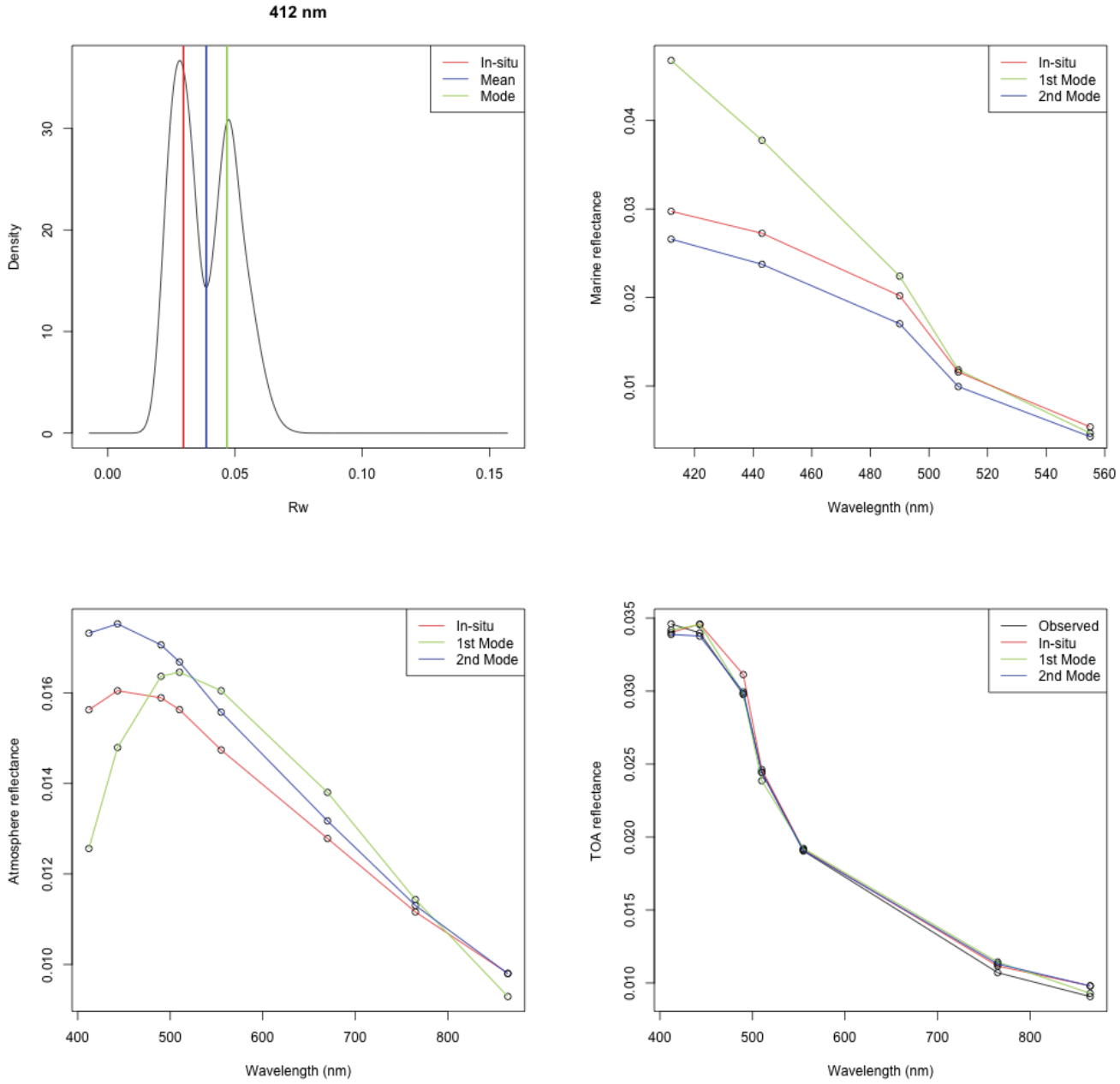

Figure 5. Analysis of a case with multiple solutions. Top-left: marginal posterior distribution of $\rho_w(412)$, with in-situ value (red), first mode (green) and mean (blue). Top-right: ρ_w spectra. Bottom-left: ρ_a spectra. Bottom-right: ρ_{TOA} spectra. Errors on ρ_{TOA} are small. Therefore, two distinct pairs (x_a, ρ_w) are found to be potential solutions which cannot be distinguished from ρ_{TOA}.